

Strongly dissimilar vortex-liquid regimes in single-crystalline NdFeAs(O,F) and (Ba,K)Fe₂As₂: A comparative study

J. Kacmarcik,^{1,2} C. Marcenat,¹ T. Klein,^{3,4} Z. Pribulova,^{2,3} C. J. van der Beek,⁵ M. Konczykowski,⁵ S. L. Budko,⁶ M. Tillman,⁶ N. Ni,⁶ and P. C. Canfield⁶

¹CEA, Institut Nanosciences et Cryogénie, SPSMS-LATEQS, 17 rue des Martyrs, 38054 Grenoble Cedex 9, France

²Centre of Low Temperature Physics IEP SAS and FS UPJŠ, Watsonova 47, 043 53 Košice, Slovakia

³Institut Néel, CNRS, B.P. 166, 38042 Grenoble Cedex 9, France

⁴Institut Universitaire de France and Université Joseph Fourier, B.P. 53, 38041 Grenoble Cedex 9, France

⁵Laboratoire des Solides Irradiés, Ecole Polytechnique, CNRS UMR7642 and CCEA/DSM/IRAMIS, 91128 Palaiseau, France

⁶Department of Physics & Astronomy and Ames Laboratory, Iowa State University, Ames, Iowa 50011, USA

(Received 29 January 2009; revised manuscript received 30 June 2009; published 21 July 2009)

The extent of the vortex-liquid state in underdoped single crystals of the oxypnictide superconductors NdFeAs(O,F) and (Ba,K)Fe₂As₂ is investigated using specific heat (C_p) and Hall-probe magnetization experiments. In both materials, the vortex liquid lies entirely in the regime where the three-dimensional lowest Landau-level (3D-LLL) approximation is valid and both systems present a very small shift in the specific heat anomaly with increasing field. The irreversibility line, defined as the onset of diamagnetic response, is very rapidly shifted toward lower temperatures in NdFeAs(O,F) but remains close to the C_p anomaly in (Ba,K)Fe₂As₂. These measurements strongly suggest that a vortex-liquid phase occupies a large portion of the mixed-state phase diagram of NdFeAs(O,F) but not in (Ba,K)Fe₂As₂. This difference can be attributed to different Ginzburg numbers Gi , the latter being about 100 times larger in NdFeAs(O,F) than in (Ba,K)Fe₂As₂. The angular dependence of the upper critical field, derived from 3D-LLL scaling of the irreversibility lines, presents deviations from the standard 3D effective-mass model in both materials with an anisotropy being about three times smaller in (Ba,K)Fe₂As₂ ($\gamma \sim 2.5$) than in Nd(F,O)FeAs ($\gamma \sim 7.5$).

DOI: [10.1103/PhysRevB.80.014515](https://doi.org/10.1103/PhysRevB.80.014515)

PACS number(s): 74.25.Ha, 74.25.Fy, 74.25.Nf, 74.25.Op

I. INTRODUCTION

The recent discovery of superconductivity at unusually high temperature (up to 56 K) in rare-earth iron oxypnictides,^{1,2} REFeAs(O_{1-x},F_x), with RE = La, Sm, Ce, Nd, Pr, Gd, Tb, Dy (the so-called 1111 phase), has been the focus of a tremendous number of theoretical and experimental work in the past few months. Superconductivity has also been observed in (Ba_{1-x},K_x)Fe₂As₂ (the so-called 122 phase) with T_c 's of up to ~ 38 K for $x \sim 0.4$.³ Both groups of materials share the particularity of having a parent composition ($x=0$) that undergoes a structural/magnetic phase transition to an orthorhombic and antiferromagnetic state. The proximity to this magnetic phase may result in large spin fluctuations and hence to the existence of an unconventional coupling mechanism.⁴ Moreover, multi-gap phenomena associated to the presence of both electron and hole pockets are also expected; angle-resolved photoemission spectroscopy⁵ as well as point-contact spectroscopy measurements have indeed suggested the presence of several gaps in both the (Ba_{1-x},K_x)Fe₂As₂ (Ref. 6) and the LaFeAs(F,O) (Ref. 7) compounds. Finally, transport measurements have rapidly indicated the existence of very large H_{c2} values, confirmed by specific-heat measurements in both the 1111 (Refs. 8 and 9) and 122 (Ref. 10) compounds. However, the influence of thermal fluctuations on the H_{c2} line remains quite unclear;¹¹ in particular, the origin of the upward curvature in the H_{c2} line deduced from transport measurements still has to be clarified.¹²

We have performed Hall-probe magnetization and specific-heat (C_p) measurements on F-doped Nd-1111 and

K-doped 122 single crystals. Superconducting anomalies were clearly observable in the heat capacity of both systems, around 34 and 26 K for NdFeAs(O,F) and (Ba,K)Fe₂As₂, respectively. Those anomalies are only very slightly shifted by a magnetic field, confirming the very high values of the upper critical fields reported in both compounds.⁸⁻¹⁰ However, a striking difference between the two systems becomes apparent when the position of the specific-heat anomaly is compared to that of the irreversibility line, defined as the onset of diamagnetic response due to flux pinning. The irreversibility line is very rapidly shifted in relatively small magnetic fields toward low temperature in NdFeAs(O,F) (see also Ref. 8), suggesting the existence of a wide vortex-liquid phase. In striking contrast, in (Ba,K)Fe₂As₂ crystals the irreversibility line tracks the C_p anomaly. This difference can be attributed to very different Ginzburg numbers $Gi \equiv \frac{1}{2}[k_B T_c / \varepsilon(0) \xi_c(0)]^2$: it turns out that Gi is about 100 times larger in Nd(O,Fe)FeAs than in (Ba,K)Fe₂As₂. In the above, $\varepsilon_0 = (\Phi_0 / 4\pi\lambda_{ab})^2$ the vortex line energy, $\xi_c = \xi_{ab} / \gamma$ and ξ_{ab} are the c -axis and ab -plane coherence lengths, γ is the anisotropy constant, and λ_{ab} is the in-plane penetration depth. We note that the presence of a narrow reversible regime lying close to the H_{c2} line can, however, not be excluded in the latter system, in agreement with recent magnetization measurements in Ba(Fe_{0.97}Co_{0.03})₂As₂.¹³

II. SAMPLE PREPARATION AND EXPERIMENTS

Single crystals of (Ba_{1-x},K_x)Fe₂As₂ were grown from a Sn flux using conventional high-temperature solution growth

techniques¹⁴ while NdFeAs(O,F) samples have been synthesized at high pressure in a cubic, multianvil apparatus.¹⁵ Both Hall-probe magnetization and C_p measurements have been performed on the same plateletlike single crystals. In the case of Nd(F,O)FeAs, these were extracted from the polycrystalline batch and have typical widths w ranging between 100 and 200 μm , and thicknesses $t \sim 30$ to 50 μm . As for (Ba,K)Fe₂As₂, the measurements were performed on small pieces [$w \sim 100$ to 300 μm and $t \sim 20$ to 30 μm] cut from a larger single crystal. Magneto-optical observations of the flux penetration have been performed on the NdFeAs(O,F) crystals. For this, a ferrimagnetic garnet indicator with in-plane anisotropy, and covered by an Al mirror layer, is placed on the superconducting crystal. Direct magneto-optical images of the magnetic-flux distribution are obtained by observing the intensity of reflected linearly polarized light using a polarized light microscope. Differential magneto-optical images are acquired by subtracting an image taken with an external applied field H from a second obtained at $H + \Delta H$; in order to improve the signal-to-noise ratio, this process is repeated 10^3 times.

The irreversibility lines (IRL) have been determined from Hall-probe magnetization measurements. For this, the samples are placed on an array of 11 miniature GaAs-based quantum-well Hall Sensors (of dimension $8 \times 8 \mu\text{m}^2$). One records the ac response of the probes in presence of a small (on the order of 1 Oe) ac field ($f \sim 213$ Hz), whence the local ac transmittivity $T'_{ac} \equiv [B_{ac}(T) - B_{ac}(4.2 \text{ K})] / [B_{ac}(4.2 \text{ K}) - B_{ac}(T \gg T_c)]$ (Ref. 16) is obtained by subtracting the response at 4.2 K and renormalizing to 1 using the data in the normal state. Full diamagnetism then corresponds to $T'_{ac} = 0$ and the irreversibility line is reached at the temperature $T_{irr}(B)$, where $T'_{ac} = 1$. In order to obtain a detailed description of the temperature and angular dependence of the irreversibility line, T'_{ac} has been measured for several values of the externally applied magnetic field H_a , for both $H_a \parallel c$ and $H_a \parallel ab$, and various intermediate field directions. The magnitude of the applied fields was $H_a = 2$ T and $H_a = 6.5$ T for (Ba,K)Fe₂As₂, and $H_a = 1.5$ T and $H_a = 3.5$ T for NdFeAs(O,F). As previously reported in Ref. 8, a small paramagnetic bump preceding the main diamagnetic jump could be observed on the probes located close to center of the sample.

Magneto-optical imaging¹⁷ of the underdoped NdFeAs(O,F) sample used for further measurements show that the specimen actually consists of two crystals joined by a grain boundary, see Fig. 1(b). Differential magneto-optical imaging [Fig. 1(a)] reveals that the crystallite in the upper right-hand corner has a sharp transition to the superconducting state at $T_c = 36.5$ K with a transition width $\Delta T_c \approx 1$ K. Similarly, the center of the larger crystallite also displays a sharp transition with a screening onset around 34 K (and complete diamagnetic screening for temperatures below 33 K, in agreement with the transmittivity measurements) but in this case superconductivity remains present in the outer ringlike shape of the crystallite up to ~ 36 K. This inhomogeneity and corresponding spread of critical temperatures ($\Delta T_c \sim 3$ K) leads to the anomalies in the transmittivity at the onset of screening. Indeed, the paramagnetic bump observed in Fig. 2(a) is due to the ringlike shape of the area of the

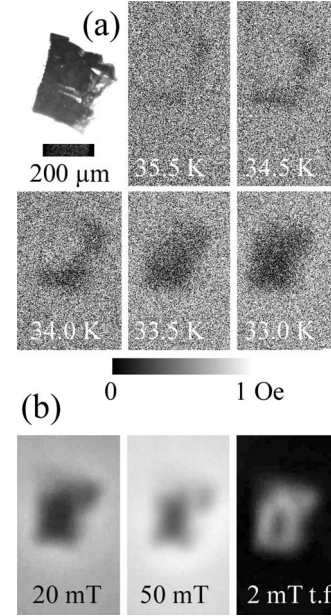


FIG. 1. (a) Polarized light image of the NdFeAs(O,F) sample used for the C_p and transmittivity measurements and five differential magneto-optical images showing the onset of diamagnetic screening of an external field of 1 Oe by this sample. The first signs of screening are observed in the upper right-hand corner at $T = 36.5$ K, diamagnetic screening is complete for $T \leq 33.0$ K. This corresponds to a transition width $\Delta T_c = 3.5$ K. The ring-shaped outer area with higher T_c leads to flux concentration in the inner region and the paramagnetic peak in Fig. 2. (b) Direct magneto-optical images of flux penetration at $T = 9.3$ K, for $H_a = 206$ Oe at 500 Oe, and the trapped flux at 26 Oe, after the application of 500 Oe. The sample consists of two crystals joined by a grain boundary. At temperatures below 32 K, the flux distributions in both crystallites are in conformity with what is expected for the Bean critical state (Refs. 18 and 19).

sample with higher T_c . Flux exclusion from that region below 36 K, together with the demagnetizing effect, first leads to a flux concentration in the central area which only becomes superconducting below 33 K. Similar effects have been observed in the (Ba,K)Fe₂As₂ platelets [see Fig. 2(b)]. Specific-heat anomalies could, however, be observed in all samples so that their quality can be qualified as reasonable. However, it would be premature to associate any broadening of the zero-field C_p transition with fluctuation effects; rather, it is the chemical inhomogeneity that leads to differences of doping in different parts of the superconducting sample. At temperatures below 32 K, the flux distribution in the NdFeAs(O,F) samples [Fig. 1(b)] conforms to the Bean critical state^{18,19} with a homogeneous critical current density j_c . This means that any flux exclusion measured by the Hall-probe technique below the IRL is due to the presence of a nonzero j_c and that the IRL is the locus of vanishing critical current.

The C_p measurements have been performed using an ac high-sensitivity technique (typically one part in 10^4). Heat was supplied to the sample by a light-emitting diode via an optical fiber and the corresponding temperature oscillations were recorded with a thermocouple which has

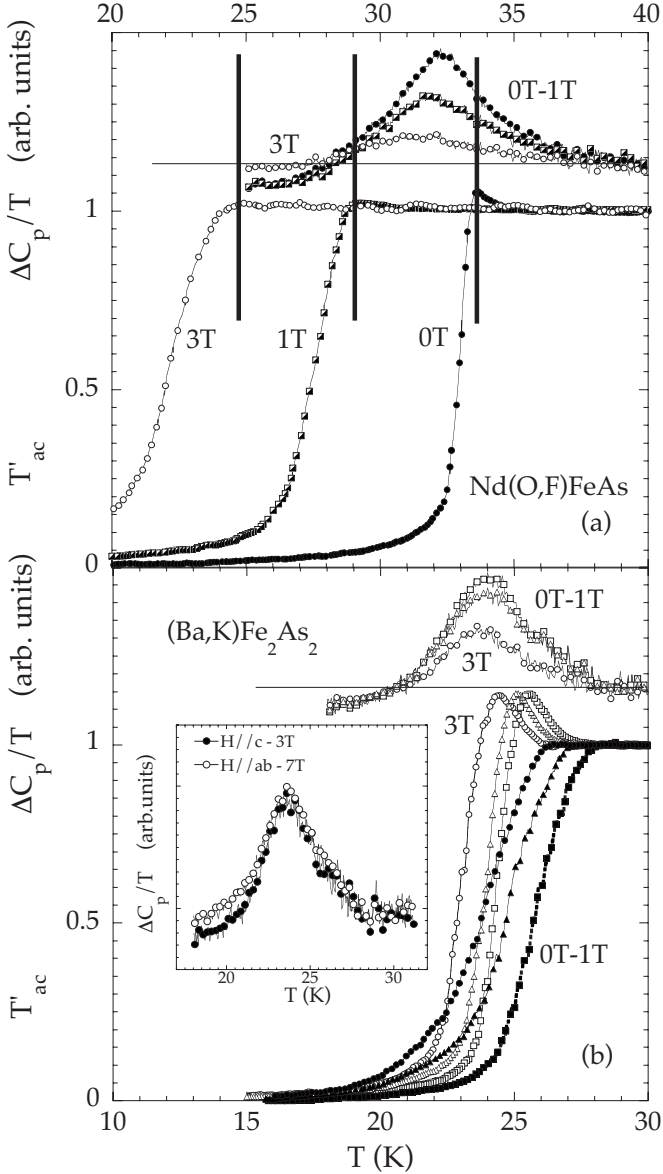


FIG. 2. (a) Temperature dependence of the ac transmittivity and specific heat for the indicated field values ($H_a||c$) in a NdFeAs(O,F) crystallite emphasizing the large difference between the position of the irreversibility line (onset of diamagnetic response at 213 Hz: vertical lines) and the specific-heat jump. (b) Similar data for $(\text{Ba,K})\text{Fe}_2\text{As}_2$, showing that the specific heat and the susceptibility data both present only a minor downward shift with applied field. The paramagnetic bump observed in both systems [although larger in $(\text{Ba,K})\text{Fe}_2\text{As}_2$ than in NdFeAs(O,F)] reflects the presence of T_c inhomogeneities in the platelets [see Fig. 1 for magneto-optical images of the NdFeAs(O,F) sample]. However the reduced shift is observed on all probe positions, open symbols corresponding to the center of the sample, and closed symbols to the sample edge (with a slightly higher T_c value). Inset: temperature dependence of the specific heat of a $(\text{Ba,K})\text{Fe}_2\text{As}_2$ crystal for $H_a||c=3\text{ T}$ (closed symbols) and $H_a||ab=7\text{ T}$ (open symbols).

been calibrated from measurements on ultrapure silicon. In NdFeAs(O,F) [respectively, $(\text{Ba,K})\text{Fe}_2\text{As}_2$], the superconducting contribution to the specific heat (ΔC_p) has been obtained by subtracting the curve at $\mu_0 H_a=7\text{ T}$ (for $H_a||c$) (re-

spectively, 14 T) from the curves obtained for lower fields. In the case of NdFeAs(O,F) , we have also subtracted a $(H_a/T)^2$ contribution accounting for the presence of a magnetic background.⁸

III. IRREVERSIBILITY LINE AND UPPER CRITICAL FIELD

Figure 1 shows that, in zero applied magnetic field, the onset of diamagnetism (when measured in the center of the sample) is close to the inflexion point of the C_p anomaly. On the other hand, the onset of the specific-heat peak well coincides with the onset of diamagnetism measured on the edge of the sample [see closed symbols in Fig. 1(b) for $(\text{Ba,K})\text{Fe}_2\text{As}_2$].

A clear difference between the two compounds appears in nonzero magnetic field. In NdFeAs(O,F) , the IRL is pushed toward substantially lower temperature when compared to the evolution of the C_p maximum: $\sim 4\text{ K}$ lower for $\mu_0 H_a=1\text{ T}$ and even $\sim 9\text{ K}$ for $\mu_0 H_a=3\text{ T}$. Thus, in this system the IRL lies well below the superconducting transition, expected in the vicinity of the C_p anomaly.²⁰ The situation is strikingly different in the case of $(\text{Ba,K})\text{Fe}_2\text{As}_2$, for which both C_p and T'_{ac} present a very small shift as a function of the magnetic field [see Fig. 2(b)]. As pointed out above, inhomogeneities of the critical temperature T_c were clearly observed in the crystals, leading, e.g., to the paramagnetic bump in the ac response of the center of the sample. Nevertheless, the same very small shift in the irreversibility line with magnetic field was observed on *all* parts of the sample. This is illustrated in Fig. 2, where open symbols show the response of the center and closed symbols that of the sample edges. We therefore conclude that, regardless of the precise composition, the irreversibility and superconducting transition lines remain close together in $(\text{Ba,K})\text{Fe}_2\text{As}_2$.

We now turn to the field dependence of the irreversibility temperature, $T_{ir}(B)$. While the IRL does correspond to the appearance of flux pinning and a bulk critical current when cooling the sample, a quantitative description of the $T_{ir}(B)$ dependence requires detailed knowledge of the flux-pinning mechanism and the summation of the elementary pinning forces acting on the vortex lattice. However, at fields exceeding the field-dependent Ginzburg criterion, $B > \frac{1}{3}T(\partial B_{c2}/\partial T)Gi(T/T_c) \sim \frac{1}{3}B_{c2}(T)$, and in the presence of only pointlike disorder,^{22,23} it can be shown that all thermodynamic and transport properties should in principle depend only on the parameter

$$Q = \frac{(1-b)(1-t^2)^{1/3}}{Gi^{1/3}(tb)^{2/3}} \quad (1)$$

as this emerges from the representation of the Ginzburg-Landau free-energy functional in terms of lowest Landau-level eigenfunctions.²²⁻²⁶ Here, $t \equiv T/T_{c0}$, with T_{c0} the mean-field critical temperature, and $b \equiv B/B_{c2}(T)$. Likewise, at fields sufficiently close to $B_{c2}(T)$, characteristic lines in the vortex phase diagram are described by the condition

$$Q = C. \quad (2)$$

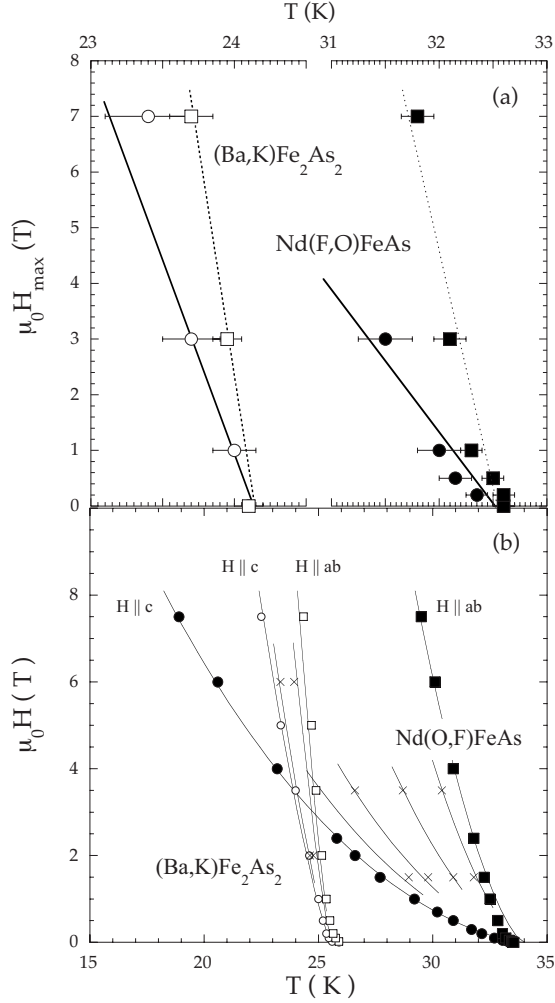


FIG. 3. (a) Position in the (B, T) plane of the maximum of the C_p anomaly. (b) Position in the (B, T) plane of the irreversibility line $T_{\text{irr}}(B)$, measured as the onset of diamagnetic response, at the center of the sample. In both panels, the circles indicate $H_a \parallel c$ while squares correspond to $H_a \parallel ab$. Closed symbols are data for $\text{NdFeAs}(\text{O,F})$ and open symbols correspond to $(\text{Ba,K})\text{Fe}_2\text{As}_2$. The crosses in Fig. 3(b) correspond to the following intermediate field directions: $\theta = 35^\circ$ (left) and 65° (right) for $(\text{Ba,K})\text{Fe}_2\text{As}_2$ and $\theta = 30^\circ, 50^\circ, 70^\circ$, and 80° (from left to right) in $\text{Nd}(\text{F,O})\text{FeAs}$. Solid lines in Fig. 3(b) are loci of constant Q , Eqs. (1) and (2), where we have used the linear slope of the solid lines in Fig. 3(a) to approximate $\partial B_{c2} / \partial$.

Examples are the vortex lattice melting line in clean superconductors which is given by the equation $F_{\text{liq}}(Q) = F_{\text{lat}}(Q)$, an equality that is satisfied for $Q \sim 8.5$.^{26–28} In disordered superconductors such as the $\text{NdFeAs}(\text{O,F})$ and $(\text{Ba,K})\text{Fe}_2\text{As}_2$ crystals under study, the IRL is the locus of minimal observable screening current due to vortex pinning. However, since all quantities related to flux pinning by uncorrelated pointlike disorder also depend on temperature and magnetic field through Q ,^{22,23} the IRL itself should also be given by the criterion [Eq. (2)], be it with a different C value than the melting line.

Figure 3(b) (solid lines) shows that the IRL in both compounds can be satisfactorily described in this manner

for all field orientations. The fit to Eq. (2) for $H_a \parallel c$ yields $CGi^{1/3} = 2.8 \pm 0.2$ for $\text{NdFeAs}(\text{O,F})$ and 0.9 ± 0.1 for $(\text{Ba,K})\text{Fe}_2\text{As}_2$, assuming that $\partial B_{c2}^c / \partial T \sim -2.5 \pm 0.3$ T/K and $\sim -6.5 \pm 0.5$ T/K in $\text{NdFeAs}(\text{O,F})$ and $(\text{Ba,K})\text{Fe}_2\text{As}_2$, respectively. Those values have been deduced from the field line corresponding to the temperature at which C_p is maximum [see circles and corresponding solid lines in Fig. 3(a)]. The value obtained in $(\text{Ba,K})\text{Fe}_2\text{As}_2$ is in excellent agreement with the C_p measurements performed by Welp *et al.*¹⁰ which yielded a clear linear temperature dependence of the $B_{c2}(T)$ line for both $H_a \parallel c$ and $H_a \parallel ab$. It is important to note that Eq. (2) can then be used to describe the IRL for all angles (other than strict alignment with the FeAs planes²⁹) using the *same* C , adjusting only the upper critical field to its value for oblique applied fields (solid lines). The corresponding value for B_{c2}^{ab} has been reported in Fig. 3(a) (dotted lines) together with the values deduced from the C_p measurements for $H_a \parallel ab$ [open and closed squares for $(\text{Ba,K})\text{Fe}_2\text{As}_2$ and $\text{NdFeAs}(\text{O,F})$, respectively], as shown a very reasonable agreement is obtained between the B_{c2} line deduced from the analysis of the irreversibility line and its direct determination from specific heat.

From Fig. 3(b), it is clear that the irreversibility lines for the two systems present rather different anisotropies. For instance, in the case of $(\text{Ba,K})\text{Fe}_2\text{As}_2$, H_{irr}^{ab} can be rescaled onto H_{irr}^c by introducing $\gamma \sim 2.5$. This anisotropy value is confirmed by the specific-heat data. Indeed, the global shape of the C_p anomaly taken at $H_a \parallel ab = 7$ T well coincides with the one at $H_a \parallel c = 3$ T [see inset of Fig. 2(b)]. Hence, we have $\gamma (= \gamma_{H_{c2}}) \sim 7/3 \sim 2.3$ in good agreement with the value reported recently by Welp *et al.*¹⁰ and Wang *et al.*³⁰ On the other hand, the irreversibility line of $\text{NdFeAs}(\text{O,F})$ presents a much stronger anisotropy $\gamma \sim 7.5$, in reasonable agreement with the value deduced from the specific-heat data.⁸ $\gamma_{H_{c2}} = 5.5 \pm 1.5$. This value is considerably larger than the one extracted from H_{c1} measurements $\gamma_{H_{c1}} \sim 4$.⁸ It is worth noting that deviations from the theoretical lines [Eq. (2)] are visible close to T_c for $H_a \parallel ab$ [see Fig. 3(b)] suggesting a decrease in $\gamma_{H_{c2}}$ close to T_c .

In order to obtain a more detailed description of $\gamma_{H_{c2}}$, we turn to the position of the irreversibility line for various field directions, $B_{\text{irr}}(T, \theta)$. These can be superposed on the irreversibility line for H_a along the c axis, B_{irr}^c , by simply rescaling the field axis: $B_{\text{irr}}(T, \theta) \rightarrow B_{\text{irr}}(T, \theta) (\partial B_{c2}^c / \partial T) / [\partial B_{c2}(\theta) / \partial T]$. The temperature derivatives $\partial B_{c2}(\theta) / \partial T$ thus obtained are shown in Fig. 4. Assuming a standard three dimensional (3D) effective-mass model for anisotropic superconductors, the angular dependence of the upper critical field should read

$$B_{c2}(\theta) = \frac{B_{c2}^c}{\varepsilon_\theta} \equiv \frac{\gamma B_{c2}^c}{\sqrt{\sin^2 \theta + \gamma^2 \cos^2 \theta}}. \quad (3)$$

The thick solid lines in Fig. 4 show the corresponding angular dependence using $\gamma_{H_{c2}} = 7.5$ for $\text{NdFeAs}(\text{O,F})$ and $\gamma_{H_{c2}} = 2.5$ for $(\text{Ba,K})\text{Fe}_2\text{As}_2$. As pointed out by Welp *et al.*,¹⁰ the experimental data show a systematic deviation from this standard behavior supporting the existence of multigap su-

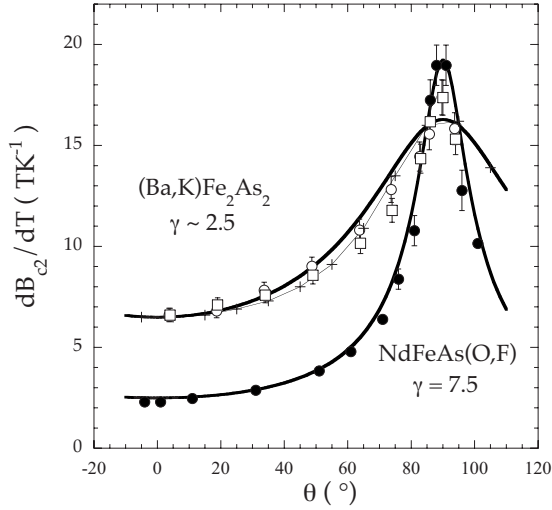


FIG. 4. Angular dependence of the upper critical field. This was extracted from fits of the IRL to Eq. (2) with a freely scaled upper critical field, for both single-crystalline NdFeAs(O,F) (●) and (Ba,K)Fe₂As₂. The data for the latter compound were taken near the sample edge (□) and near the sample center (○). The crosses correspond to the values deduced from specific-heat measurements in Ref. 10. Thick solid lines correspond to the 3D effective-mass model for the indicated anisotropy factors γ .

perconductivity as previously observed in MgB₂.³¹ A similar effect has also been reported by Jaroszynski *et al.*¹² from transport measurements. These authors, however, introduced different γ values to describe the behavior at different R/R_n values.

IV. GINZBURG NUMBER

The first penetration field H_p has been deduced by measuring the remanent field (B_{rem}) in the sample after applying an external field H_a and sweeping the field back to zero. From there, H_{c1} was estimated introducing a demagnetization factor of the form $B_{c1} \approx \mu_0 H_p / \tanh(\sqrt{\alpha d/2w})$ in order to take the edge effects associated to the nonelliptical shape of the crystallites into account.³² Taking an average α value ~ 0.5 ($\alpha \sim 0.36$ in strips and ~ 0.67 in disks³³) we obtained $B_{c1}^c(0) \sim 120 \pm 30$ G in NdFeAs(O,F);⁸ similar measurements lead to $B_{c1}^c(0) \sim 400 \pm 100$ G in (Ba,K)Fe₂As₂.

The lower critical field is related to the penetration depth through the relation $B_{c1}^c = \Phi_0 / (4\pi\lambda_{ab}^2) [\ln(\kappa) + c(\kappa)]$,

where $\kappa = \lambda_{ab} / \xi_{ab}$ and $c(\kappa)$ a κ -dependent function tending toward ~ 0.5 for large κ values. Taking $H_{c2}^c(0) \sim 55$ T for NdFeAs(O,F) and ~ 120 T and (Ba,K)Fe₂As₂, one gets $\lambda_{ab}(0) \sim 270 \pm 40$ nm in the first material, which is slightly larger than the value of ~ 200 nm obtained by muon spin-relaxation data on samples with higher T_c values,³⁴ and $\lambda_{ab} \sim 140 \pm 20$ nm in (Ba,K)Fe₂As₂. The latter value agrees with those previously reported for this system, which range from $\lambda_{ab} \sim 110$ nm (Ref. 35) to ~ 170 nm (Ref. 10).

The value of the Ginzburg number and other parameters deduced from our measurements are reported in Table I. They are compared with those obtained on optimally doped YBaCuO (Ref. 21) as well as with (Ba,K)BiO₃ (Ref. 36) or MgB₂ (Ref. 37) with similar T_c values. The Ginzburg number is clearly about two orders of magnitude larger in Nd-FeAs(O,F) than in (Ba,K)Fe₂As₂. By consequence, the vortex-liquid phase should occupy a much larger portion of the (B, T) phasediagram, in agreement with our measurements which clearly a much larger separation between the irreversibility line and the superconducting-to-normal transition in the former system. The smaller effects of thermal fluctuations in (Ba,K)Fe₂As₂ have also been emphasized by Welp *et al.*,¹⁰ who pointed out that those effects are further reduced in field due to the very large values of B_{c2} . However, our measurements suggest that a small liquid phase is still present in (Ba,K)Fe₂As₂. This is in contrast with the cubic (K,Ba)BiO₃ compound that has a similar Gi value²⁰ and therefore emphasizes the importance of even a “modest” anisotropy in the vortex depinning process—this is because the tilt modulus of the vortex lattice scales as $1/\gamma^2$.³⁸

It is worth noting that introducing the Gi values in the $CGi^{1/3}$ constants used to fit the irreversibility lines leads to very similar C values for the two materials, i.e., $C = 11 \pm 3$ and 15 ± 5 in Nd(F,O)FeAs and (Ba,K)Fe₂As₂, respectively. Those values, larger than the locus of vortex lattice melting in clean superconductors, which occurs at $Q = C \sim 8.5$, indicate that disorder plays a significant role in the physical properties of the vortex system in both materials [especially in (Ba,K)Fe₂As₂]. Indeed, the presence of quenched disorder is expected to lead to a downward shift of the melting line²³ which corresponds to an increase in C in Eq. (3).

V. CONCLUSION

Both the (Ba,K)Fe₂As₂ and Nd(F,O)FeAs systems present a very small shift of the specific-heat anomaly with

TABLE I. London penetration depth (λ_{ab} in nm), Coherence length (ξ_{ab} in nm), anisotropy (γ), critical temperature (T_c in K), line energy ($\varepsilon_0 \xi_c$ in K), and Ginzburg number (Gi) in NdFeAs(O,F) and (Ba,K)Fe₂As₂ crystals in comparison with the high T_c cuprate YBa₂Cu₃O₇, (Ba,K)BiO₃, and MgB₂.

Compound	λ_{ab}	ξ_{ab}	γ	T_c	$\varepsilon_0 \xi_c$	Gi
YBaCuO	~ 120	~ 1.4	7	92	220	2×10^{-3}
NdFeAs(O,F)	270 ± 40	~ 2.4	7.5	35	100 ± 30	$8.10^{-3} - 4.10^{-2}$
(Ba,K)Fe ₂ As ₂	140 ± 20	~ 1.6	2.5	28	600 ± 200	$1 - 5 \times 10^{-4}$
(Ba,K)BiO ₃	~ 280	~ 3	1	32	800	3×10^{-4}
MgB ₂	~ 50	~ 10	5	39	16 000	10^{-6}

increasing field, confirming the very high H_{c2} values reported previously. However, whereas the irreversibility line is very rapidly shifted in magnetic field toward low temperature in NdFeAs(O,F), this line remains close to the C_p anomaly in (Ba,K)Fe₂As₂. Our measurements therefore strongly suggest the existence of a much wider vortex-liquid phase in NdFeAs(O,F) than in (Ba,K)Fe₂As₂. This difference can be attributed to very different values of the Ginzburg parameter, Gi being about 100 times larger in NdFeAs(O,F) ($Gi \sim 10^{-2}$) than in (Ba,K)Fe₂As₂ ($Gi \sim 10^{-4}$). Nevertheless, the depinning mechanism leading to the irreversibility line is similar in both compounds, as attested by the similar loci of the lowest Landau-level parameter Q at which the IRL occurs. It is worth mentioning that, in contrast to (Ba,K)Fe₂As₂, NdFeAs(O,F) also has a magnetic-moment bearing rare-earth atom in its structure.

The influence of this local moment on the magnetic properties of the mixed state still has to be clarified.

ACKNOWLEDGMENTS

We are most obliged to V. Mosser of ITRON, Montrouge, for the development of the Hall sensors used in this study. Work at the Ames Laboratory was supported by the Department of Energy, Basic Energy Sciences under Contract No. DE-AC02-07CH11358. Z.P. thanks the Slovak Research and Development Agency under the Contract No. LPP-0101-06. C.M. and J.K. thank the 6th Framework Programme MCA Transfer of Knowledge project under ExtreM No. MTKD-CT-2005-03002. T.K., Z.P., and M.K. thank the ANR-MICROMAG BLAN07-2 under Contract No. 26280 for financial support.

-
- ¹Y. Kamihara, T. Watanabe, M. Hirano, and H. Hosono, *J. Am. Chem. Soc.* **130**, 3296 (2008).
- ²C. Wang, L. Li, S. Chi, Z. Zhu, Z. Ren, Y. Li, Y. Wang, X. Lin, Y. Luo, S. Jiang, X. Xu, G. Cao, and Z. Xu, *EPL* **83**, 67006 (2008).
- ³M. Rotter, M. Tegel, and D. Johrendt, *Phys. Rev. Lett.* **101**, 107006 (2008).
- ⁴L. Boeri, O. V. Dolgov, and A. A. Golubov, *Phys. Rev. Lett.* **101**, 026403 (2008); I. I. Mazin, D. J. Singh, M. D. Johannes, and M. H. Du, *ibid.* **101**, 057003 (2008).
- ⁵H. Ding, P. Richard, K. Nakayama, K. Sugawara, T. Arakane, Y. Sekiba, A. Takayama, S. Souma, T. Sato, T. Takahashi, Z. Wang, X. Dai, Z. Fang, G. F. Chen, J. L. Luo, and N. L. Wang, *EPL* **83**, 47001 (2008).
- ⁶P. Szabo, Z. Pribulova, G. Pristas, S. L. Bud'ko, P. C. Canfield, and P. Samuely, *Phys. Rev. B* **79**, 012503 (2009).
- ⁷R. S. Gonnelli, D. Daghero, M. Tortello, G. A. Ummarino, V. A. Stepanov, J. S. Kim, and R. K. Kremer, *Phys. Rev. B* **79**, 184526 (2009).
- ⁸Z. Pribulova, T. Klein, J. Kacmarcik, C. Marcenat, M. Konczykowski, S. L. Budko, M. Tillman, and P. C. Canfield, *Phys. Rev. B* **79**, 020508 (2009).
- ⁹U. Welp, R. Xie, A. E. Koshelev, W. K. Kwok, P. Cheng, L. Fang, and H. H. Wen, *Phys. Rev. B* **78**, 140510(R) (2008).
- ¹⁰U. Welp, R. Xie, A. E. Koshelev, W. K. Kwok, H. Q. Luo, Z. S. Wang, G. Mu, and H. H. Wen, *Phys. Rev. B* **79**, 094505 (2009).
- ¹¹A. Yamamoto, J. Jaroszynski, C. tarantini, L. Balicas, J. Jiang, A. Gurevich, D. C. Larbalestier, R. Jin, A. S. Sefat, M. A. McGuire, B. C. Sales, D. K. Christen, and D. mandrus, *Appl. Phys. Lett.* **94**, 062511 (2009).
- ¹²J. Jaroszynski, F. Hunte, L. Balicas, Youn-Jung Jo, I. Raicevic, A. Gurevich, D. C. Larbalestier, F. F. Balakirev, L. Fang, P. Cheng, Y. Jia, and H. H. Wen, *Phys. Rev. B* **78**, 174523 (2008).
- ¹³R. Prozorov, N. Ni, M. A. Tanatar, V. G. Kogan, R. T. Gordon, C. Martin, E. C. Blomberg, P. Prommapan, J. Q. Yan, S. L. Budko, and P. C. Canfield, *Phys. Rev. B* **78**, 224506 (2008).
- ¹⁴N. Ni, S. L. Budko, A. Kreyssig, S. Nandi, G. E. Rustan, A. I. Goldman, S. Gupta, J. D. Corbett, A. Kracher, and P. C. Canfield, *Phys. Rev. B* **78**, 214515 (2008).
- ¹⁵M. Tillman *et al.*, (unpublished).
- ¹⁶J. Gilchrist and M. Konczykowski, *Physica C* **212**, 43 (1993).
- ¹⁷L. A. Dorosinskii, M. V. Indenbom, V. I. Nikitenko, Yu. A. Ossip'yan, A. A. Polyanskii, and V. K. Vlasko-Vlasov, *Physica C* **203**, 149 (1992).
- ¹⁸C. P. Bean, *Phys. Rev. Lett.* **8**, 250 (1962).
- ¹⁹E. Zeldov, J. R. Clem, M. McElfresh, and M. Darwin, *Phys. Rev. B* **49**, 9802 (1994).
- ²⁰Note that in disordered superconductors the maximum of the specific heat by no means needs to coincide with the upper critical field; see Ref. 21.
- ²¹C. J. van der Beek, M. Konczykowski, L. Fruchter, R. Brusetti, T. Klein, J. Marcus, and C. Marcenat, *Phys. Rev. B* **72**, 214504 (2005).
- ²²G. P. Mikitik and E. H. Brandt, *Phys. Rev. B* **64**, 184514 (2001).
- ²³G. P. Mikitik and E. H. Brandt, *Phys. Rev. B* **68**, 054509 (2003).
- ²⁴D. J. Thouless, *Phys. Rev. Lett.* **34**, 946 (1975).
- ²⁵R. Ikeda, T. Ohmi, and T. Tsuneto, *J. Phys. Soc. Jpn.* **58**, 1377 (1989).
- ²⁶S. Hikami, A. Fujita, and A. I. Larkin, *Phys. Rev. B* **44**, 10400 (1991).
- ²⁷D. P. Li and B. Rosenstein, *Phys. Rev. Lett.* **86**, 3618 (2001); B. Rosenstein, *Phys. Rev. B* **60**, 4268 (1999).
- ²⁸Note that this condition is mathematically equivalent to writing a Lindemann criterion for the vortex lattice melting process—see Eqs. (13) and (23) in Ref. 23 for $h_m \rightarrow 1$. In this respect, it may be noted that a very good approximation of the melting line in clean superconductor is given by a simple $(1-t^2)^\alpha$ formula for $t=T/T_c > 0.5$ with $1.24 < \alpha < 1.59$ for $0.001 < Gi < 0.01$ (Ref. 23) (as often observed for the melting line in high T_c oxides). This law is well verified in both compounds with $\alpha \sim 1.50(\pm 0.05)$ and $\alpha \sim 1.3(\pm 0.1)$ in NdFeAs(F,O) and (Ba,K)Fe₂As₂, respectively, emphasizing the larger Gi value in the former system.
- ²⁹G. Blatter, M. V. Feigel'man, V. B. Geskenbein, A. I. Larkin, and V. M. Vinokur, *Rev. Mod. Phys.* **66**, 1125 (1994).
- ³⁰Zhao-Sheng Wang, Hui-Qian Luo, Cong Ren, and Hai-Hu Wen, *Phys. Rev. B* **78** 140501(R) (2008).
- ³¹A. Rydh, U. Welp, A. E. Koshelev, W. K. Kwok, G. W. Crabtree,

- R. Brusetti, L. Lyard, T. Klein, C. Marcenat, B. Kang, K. H. Kim, K. H. P. Kim, H.-S. Lee, and S.-I. Lee, *Phys. Rev. B* **70**, 132503 (2004).
- ³²E. H. Brandt, *Phys. Rev. B* **59**, 3369 (1999); E. Zeldov, A. I. Larkin, V. B. Geshkenbein, M. Konczykowski, D. Majer, B. Khaykovich, V. M. Vinokur, and H. Shtrikman, *Phys. Rev. Lett.* **73**, 1428 (1994).
- ³³A detailed analysis on MgB₂ samples showed that all measured samples fell within those two (strips and disks) limits; L. Lyard, T. Klein, J. Marcus, R. Brusetti, C. Marcenat, M. Konczykowski, V. Mosser, K. H. Kim, B. W. Kang, H. S. Lee, and S. I. Lee, *Phys. Rev. B*, **70**, 180504(R) (2004).
- ³⁴R. Khasanov, H. Luetkens, A. Amato, H. H. Klauss, Z. A. Ren, J. Yang, W. Lu, and Z. X. Zhao, *Phys. Rev. B* **78**, 092506 (2008).
- ³⁵C. Ren, Z. S. Wang, H. Q. Luo, H. Yang, L. Shan, and H.-H. Wen, *Phys. Rev. Lett.* **101**, 257006 (2008).
- ³⁶S. Blanchard, T. Klein, J. Marcus, I. Joumard, A. Sulpice, P. Szabo, P. Samuely, A. G. M. Jansen, and C. Marcenat, *Phys. Rev. Lett.* **88**, 177201 (2002); I. Joumard, J. Marcus, T. Klein, and R. Cubitt, *ibid.* **82**, 4930 (1999).
- ³⁷L. Lyard, P. Samuely, P. Szabo, T. Klein, C. Marcenat, L. Paulius, K. H. P. Kim, C. U. Jung, H. S. Lee, B. Kang, S. Choi, S. I. Lee, J. Marcus, S. Blanchard, A. G. M. Jansen, U. Welp, G. Karapetrov, and W. K. Kwok, *Phys. Rev. B* **66**, 180502(R) (2002); T. Klein, L. Lyard, J. Marcus, Z. Holanova, and C. Marcenat, *ibid.* **73**, 184513 (2006).
- ³⁸A. Sudbø and E. H. Brandt, *Phys. Rev. Lett.* **66**, 1781 (1991); *Phys. Rev. B* **43**, 10482 (1991).